Anisotropic In-plane Conductivity and Dichroic Gold Plasmon Resonance in Plasma Assisted ITO Thin Films e-Beam Evaporated at Oblique Angles

Julian Parra-Barranco†, Fran J. Garcia-Garcia†, Victor Rico†, Ana Borrás†, Carmen López-Santos†, Fabian Frutos&, Angel Barrranco†, Agustin R. Gonzalez-Elipe*†

†Nanotechnology on Surfaces Laboratory, Instituto de Ciencia de Materiales de Sevilla, Consejo Superior de Investigaciones Científicas (CSIC)-Universidad de Sevilla. c/Américo Vespucio 49, Sevilla 41092, ES, Spain.

&Applied Physics Department, E.T.S. Ingeniería Informática, University of Sevilla, Avd. Reina Mercedes s/n, Sevilla 41012, Spain

ABSTRACT

ITO thin films have been prepared by electron beam evaporation at oblique angles (OA), directly and while assisting their growth with a downstream plasma. The films microstructure, characterized by scanning electron microscopy, atomic force microscopy and glancing incidence small angle X-ray scattering, consisted of tilted and separated nanostructures. In the plasma

assisted films, the tilting angle decreased and the nanocolumns became associated in the form of bundles along the direction perpendicular to the flux of evaporated material. The annealed films presented different in-depth and sheet resistivity as confirmed by scanning conductivity measurements taken for the individual nanocolumns. In addition, for the plasma assisted thin films, two different sheet resistance values were determined by measuring along the nanocolumn bundles or along the perpendicular direction. This in-plane anisotropy induces the electrochemical deposition of elongated gold nanostructures. The obtained Au-ITO composite thin films were characterized by anisotropic plasmon resonance absorption and a dichroic behavior when examined with linearly polarized light.

INTRODUCTION

Due to its excellent conductivity, high optical transmission and the relatively easy up-scaling of manufacturing processes, Indium tin oxide (ITO) is a key transparent electronic material.[1] Only its cost and the relative scarcity of indium have prompted the search for other alternative transparent and conductive (TCO) films.[2] ITO thin films have been prepared by a large variety of procedures including wet (i.e., sol-gel, spray, dip-coating, etc.[3,4]) or dry, (i.e., vacuum and plasma) methods of deposition, these latter including e-beam evaporation or magnetron sputtering.[5–8] Recently, porous nanostructured ITO thin films and related stacked nanostructures have been prepared by deposition at oblique angles (OAD thin films).[9–13] By this manufacturing process, the substrates form an oblique angle with respect to the flux direction of the deposition material usually generated by e-beam or magnetron sputtering.[14–16] Metals,[17,18] oxides,[19–22] semiconductors[23,24] and molecular materials[25] have been prepared in the form of thin films by using this methodology. Their microstructure consists of tilted nanocolumns which, extending

from the interface with the substrate up to the surface, confer the films outstanding optical, adsorption or magnetic properties.[26–32]OAD-ITO nanostructured layers have been also stacked in the form of 1D photonic crystals[33,34] that depict singular Bragg reflection and conductivity performances.[35,36] On the other hand, branched ITO nanostructures have been also prepared by OA evaporation under conditions inducing a vacuum liquid-solid (VLS) growth.[37–41] In these systems the electrical conductivity is expected to be higher along the direction of the specific elements in their nanostructure.

In the present work we have developed an experimental strategy consisting of plasma assisting the growth of e-beam OAD ITO thin films. In literature, OAD thin films have been grown under the effect of a beam of accelerated ions.[42] Once formed, compact ITO thin films have been also subjected to plasma etching to induce the growth of nanopillar structures.[12] However, to our knowledge, there are no previous essays where a plasma is used to assist the growth of e-beam OAD thin films during deposition. Besides describing the experimental procedure, we present here a thorough characterization of the OAD-ITO films prepared both by direct e-beam evaporation or by assisting the deposition with Ar or O_2 plasmas supplied with a low pressure plasma source. Scanning electron microscopy (SEM), topographic atomic force and electrical scanning microscopy (AFM), gracing incidence small angle X-ray scattering (GISAXS), besides sheet and in-depth conductivity measurements have been utilized for the characterization analysis of the samples. It will be shown that, besides changes in the nanocolumns orientation, an outstanding effect of plasma assisting the film growth is the bundling association of the individual nanocolumns[14,43] that define a preferential direction rendering anisotropic in-plane conductivity. A preliminary discussion about this anisotropic bundling association of nanocolumns under the action of a plasma has been carried out within the frame of the trapping

mechanism concept[44,45] recently proposed by us to account for the tilting angle of nanocolumns beyond the heuristic tangent and cosine rules.[46]

To illustrate the possibilities of application of this type of anisotropy in microstructure and electrical properties, we propose the preparation of dichroic thin films formed by the electrochemical deposition of gold nanostructures on the anisotropic ITO films. In previous works we have shown that anisotropic gold or silver nanostructures presenting a dichroic plasmon resonance behavior can be prepared by different chemical or physical methods making use of a template effect of the bundles developed in OAD SiO_2 thin films.[47,48] In the present work, contrary to the electrochemical deposition of isotropic and spherical gold nanoparticles found on conventional ITO films,[49,50] a surface template effect of the plasma assisted OAD-ITO layers has prompted the electrochemical deposition of anisotropic gold nanostructures with a clear dichroic behavior of their surface plasmon resonance absorption.

EXPERIMENTAL

Thin film preparation

ITO thin films have been prepared in an e-beam evaporator set-up previously described for the OAD of TiO_2[19] and SiO_2[45] thin films. In this system, a large number of specimens can be prepared simultaneously at different zenithal angles (α) of evaporation. Values of α= 60º, 70º, 80º and 85º have been used for the films deposited in the absence of plasma, while only α=80º was used when assisting the film growth with a plasma. This limitation stems from geometrical constrains of the deposition chamber where this value of α is determined by the position of the plasma source. A design of the experimental set-up used for the plasma assisted OAD of thin films is shown in Figure 1. The utilized plasma source was a microwave (MW) operated device

(2.45 GHz, 460 W) consisting of a bell jar supplied through its upper part with the plasma gas (O_2, Ar and mixtures of these two gases). A pressure of 10^{-4} torr was always kept in the interior of the deposition chamber during e-beam evaporation, either in the presence or in the absence of the plasma. Although no direct measurement of the pressure is possible in the bell jar of the plasma source, a value of $3\text{-}5\text{x}10^{-4}$ torr is expected in its interior. An evaporation rate of 0.7-1.0 A s^{-1} was set at the sample position. The plasma source was ignited before moving away a shutter that was covering the substrates for their protection.

The ITO target, consisting of pellets supplied by Kurt J. Lesker. (In_2O_3/SnO_2 90%/10% (w/w)), were placed in a graphite crucible for e-beam bombardment. OAD thin films were prepared on silicon wafers and quartz plates for specific characterization essays. Commercial ITO plates, supplied by VisionTek Systems Ltd (4 ohms/sq ITO 370 nm thick ITO), were used as substrates for the OAD of ITO films intended for the electrochemical deposition of gold and other characterization studies.
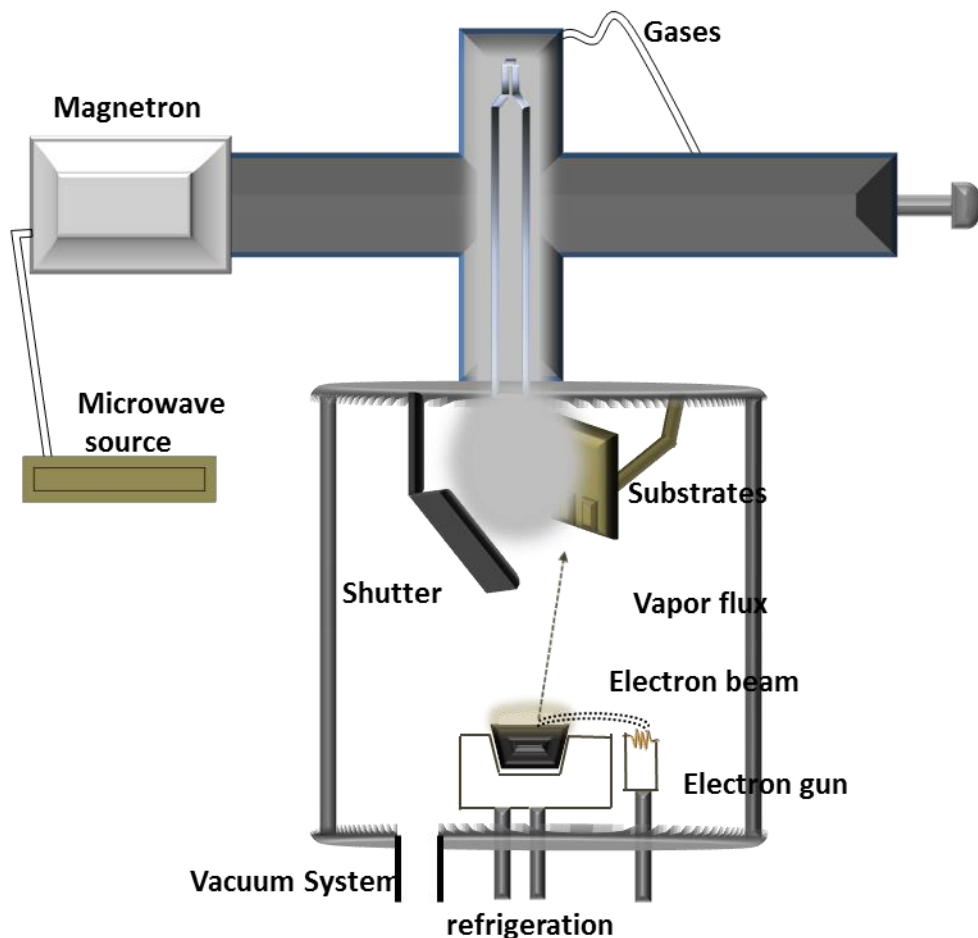
Figure 1. Scheme of the experimental set up used for the e-beam deposition of ITO films in an OAD configuration while assisting their growth with a downstream plasma.

Thin films characterization

The microstructure of the films was characterized for the samples prepared on silicon wafers. They were diced for their lateral examination with a SE microscope HITACHI-S-5200 operated at 2KV.

GISAXS characterization studies were carried out at the P03 synchrotron beam-line of the PETRA III facility (Hamburg), using a wavelength of 0.168 Å and a sample to detector distance of 2.5 m.[51] The scattering signal was recorded with a 2D detector (Pilatus 300k fast with 172 µm pixel size). For each sample two different patterns were recorded, either by placing the films

oriented with the tilted nanocolumns facing the polarization plane of the X-ray beam or in the direction perpendicular to it. Only spectra for this latter configuration, where the X-ray impinges perpendicular to the plane containing the tilted nanocolumnar structure, will be presented here for discussion. Details about data acquisition and calculation can be found in previous publications.[19,52,53] All examined films had a similar thickness of 500 nm.

In-depth elemental profiles and average Sn/In ratios were determined by Rutherford Back Scattering (RBS). The spectra were taken in a 3 MeV tandem accelerator at the CNA (Sevilla, Spain) with a proton beam of 1.5 MeV. Back scattered particles were recollected with a tilted Si detector at 165º for the sample holder tilted by 7º with respect to the beam. The RBS spectra were simulated with the SIMRNA software.[54]

AFM characterization of the surface of the films was carried out with a Nanotec Dulcinea microscope (Spain). Scanning conductivity measurements were carried out with a current sensing module supplied with a conductive tip NT-MDT with a gold cover. The diameter of the conductive tip was 70 nm and it presented a resonance frequency of 190-325 KHz and a force constant of 5.5-22.5 N/m.

Electrical measurements

Cross section and sheet resistance (although this term usually applies to homogeneous and compact thin films, we keep it here for simplicity) measurements were done with a Kietley 2635A System SourceMeter. For cross section measurements, OAD thin films were grown on commercial ITO plates. Electrical measurements were done between the conductive substrate and a copper contact on the surface. Films grown on a quartz plate were used for sheet resistance determination. The measurements were done between two copper contacts deposited on the surface. These electrodes were spherical conductive adhesive copper spots of 3 mm diameter

separated by 8 mm. The I-V curves were obtained with a compliance of 10^{-3} A. The used voltage ranged between $-4*10^{-3}$ to $4*10^{-3}$ V.

Electrochemical deposition of gold

Films with a ~1.5 cm^2 working area were polarized at room temperature in a rectangular three-electrode electrochemical cell made of quartz. A saturated Ag/AgCl and a platinum foil were employed as reference and counter electrodes, respectively. Electrochemical measurements were performed with a computer controlled Autolab PGSTAT30 potentiostat. Gold was electrodeposited by the application of a constant current density (-300 μA cm^{-2}) during 400 seconds in an aqueous solution of 0.1 M HAuCl4 in acetone as reported in refs.[55,56]

UV-Vis transmittance spectra were recorded during and after the electrochemical measurements with a DH-2000 light source equipped with halogen and deuterium lamps and a QE65000 high-resolution spectrophotometer from Ocean Optics.

RESULTS

Morphology of OAD and OAD plasma assisted ITO thin films

Figure 2 shows normal and cross section SEM micrographs of a series of ITO thin films prepared in the absence of plasma at different zenithal angles from 60º to 85º under a pressure of 10^{-4} torr of O_2. These micrographs show that the evaporated material aggregates in the form of individual tilted nanocolumns extending from the interface with the substrate to the surface of the film. As the film thickness increases, these nanocolumns slightly bend to higher angles with respect to the perpendicular to the surface. Although this bending precludes a straightforward determination of the orientation angle (β) of nanocolumns for the whole film thickness, a rough estimation of β approaching the bended nanocolumns to straights gives average values around

45º for all the films, with negligible changes from $\beta \sim 41º$ for $\alpha=60º$ to $\beta \sim 46º$ for $\alpha=85º$. These values contrast with the tilting angles determined for thinner films of approximately 200 nm when the nanocolumns are not yet bended. In this case, well defined β values varying from ca. 25º ($\alpha=60º$) to 43º ($\alpha=85º$) can be determined.[44] These tilting angles do not agree with the predictions of the heuristic tangent rule,[57] a discrepancy that we have recently explained by assuming a trapping process for the ballistic particles flying close to the deposited nanostructures.[44] Another remarkable feature of these OAD ITO nanostructures is that they are rather smooth and do not depict the typical feather-like termination characteristic of the nanocolumns of TiO_2 and other oxides evaporated in an OAD configuration.[19,21] Other authors have obtained similar thin film microstructures for e-beam OAD ITO films.[11,12]

When the growing films were exposed to plasma at a similar pressure of 10^{-4} torr, the morphology of the films experienced significant changes that affected the shape, size, agglomeration and tilting angle of the nanocolumns. Figure 3 shows a series of normal and cross section SEM micrographs corresponding to ITO thin films prepared at a zenithal angle of 80º in the presence of several types of plasmas. As explained in the experimental section other evaporation angles were not possible because of experimental restrictions. An outstanding characteristic of the microstructure of these plasma assisted OAD thin films is that the nanocolumns are not isolated but associate in the form of bundles[14,43,47,48,58] that stretch along a direction perpendicular to the incoming flux of evaporated material. Bundling association of nanocolumns in OAD thin films is a common phenomenon previously reported for a large variety of materials.[14,43,58] Another important characteristic of the plasma assisted OAD-ITO thin films is that the tilting angle β stays around 30 º, varying only slightly with the type of plasma gas (see Table 1). A different growing mechanism for the plasma assisted ITO OAD thin films is

clearly evidenced in Figure 4 showing a cross section micrograph of a stacked bilayer of ITO films sequentially deposited in the absence (bottom) and in the presence (top) of an oxygen plasma.
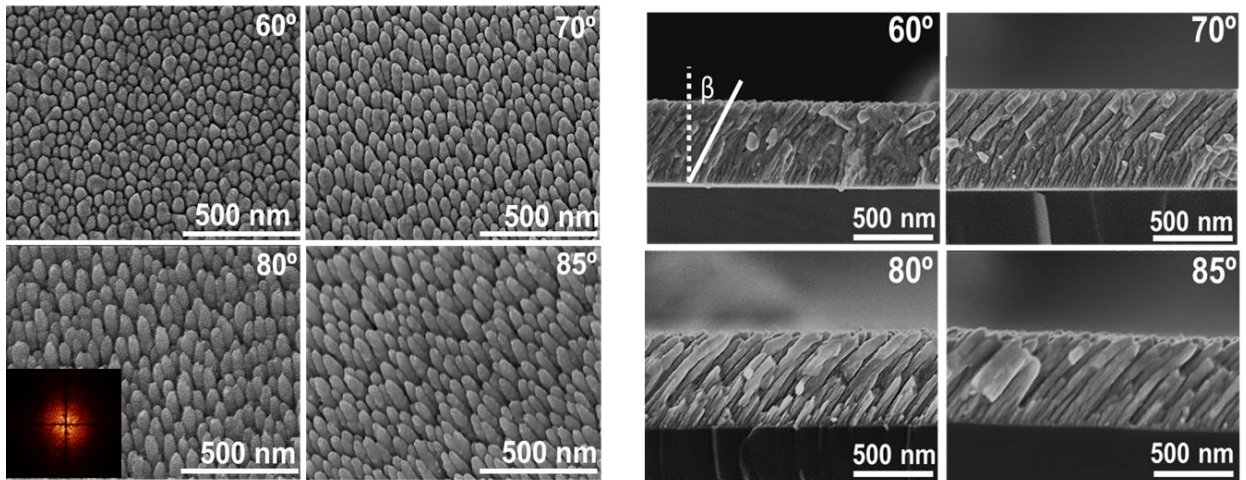

Figure 2. Normal (left) and cross section (right) SEM micrographs of ITO thin films prepared by OAD at the indicated zenithal angles from 60º to 85º in the presence of an oxygen pressure of 10^{-4} torr. The inset in the 80º normal SEM micrograph is the FFT of this image.
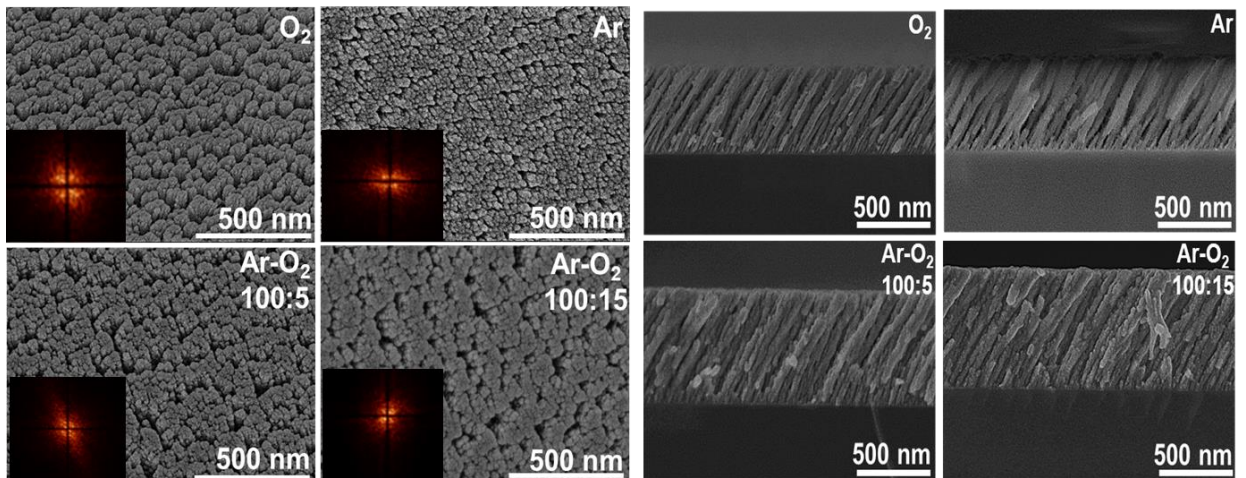
Figure 3. Normal (left) and cross section (right) SEM micrographs of ITO thin films prepared by OAD at a zenithal angle of 80º while assisting their growth with different types of plasma at an overall pressure of 10-4 torr. The insets in the normal SEM micrographs correspond to the FFT diagrams obtained from the normal SEM micrographs in each case (see text).
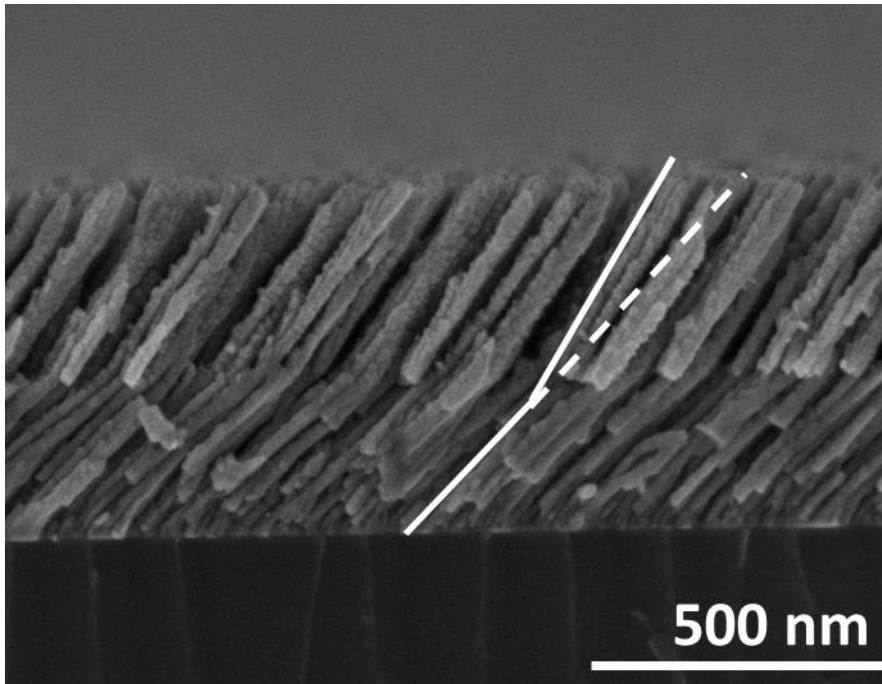

Figure 4. SEM cross section micrograph of a ITO bilayer prepared by OAD, where the bottom layer has been prepared in the absence of plasma and the top layer by assisting the growth with a plasma of oxygen.

Table 1. Tilting angle of nanocolumns in the OAD ITO films grown by assisting the thin film growth with different plasmas.

Plasma type	Tilting angle β
O_2	30º
Ar	24º
Ar:O2(100:5)	26º
Ar:O2 (100:15	25º
ITO OAD 80º	46º

GISAXS analysis of OAD thin films has demonstrated to be a very powerful technique to retrieve information about possible anisotropy in the bulk and to determine the existence of specific correlation distances between the nanocolumnar features.[52,53] Figure 5 shows a series of GISAXS patterns of ITO thin films deposited at different zenithal angles in the absence of plasma and for the plasma assisted films deposited at α=80º. Except for the pattern of the ITO compact thin film (i.e., a commercial ITO plate), the patterns recorded for the OAD films are characterized by an asymmetric shape indicative of a tilted orientation of the nanocolumns with respect to the film surface.[52,53] Moreover, the development in all cases of well-defined maxima proves the existence of specific correlations distances between the basic microstructural units of the films (i.e., the existence of a repetitive distance that, on average, separate these microstructural units). Table 2 summarizes the values of these correlation distances for the examined films and show that the average separation between nanostructures in the O_2 plasma assisted films is slightly larger than in the evaporated films or in the films grown in the presence of a plasma of Ar. Since the GISAXS values are averaged through the whole thickness of the

films and the nanocolum width usually increases with this parameter[59,60] it is expected that the surface periodicity deduced from an AFM analysis of roughness defined by the nanocolumn termination differs from the GISAXS correlation distances. This is in fact shown by the values of the grain sizes estimated from the Bearing plots of the AFM images (see supporting information S1) that are higher than GISAXS correlation distances (see Table 1). Similar differences were found in a previous work for TiO_2 OAD thin films.[19]
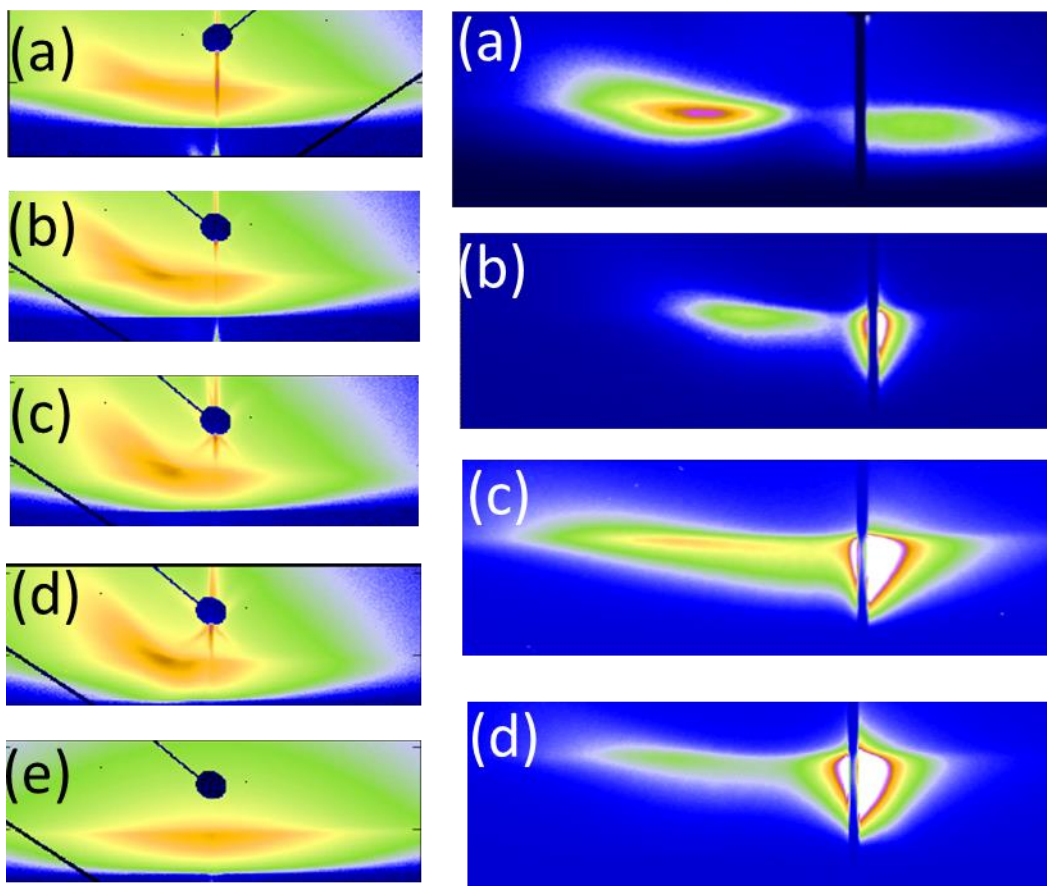

Figure 5. GISAXS patterns of ITO thin films. (left) Thin films deposited at different zenithal angles α in the absence of plasma: 60º (a), 70º (b), 80º (c), 85º (d), compact ITO thin films (e). (right) Thin films deposited at α=80º under the assistance of the following plasmas: Ar (a), O2

(b), Ar:O2 (100:5) (c), Ar:O2 (100:15) (d). The color scale is indicative of the scattering intensity.

Table 2. Correlation distances determined from GISAXS patterns and surface periodicity determined from the AFM images of the same samples.

Zenithal deposition angle/type of plasma	GISAXS correlation distances (nm)	Averaged urface grain sizes deduced from AFM images (nm)
60º	11	-
70º	14	-
80º	16	25
85º	18	-
80º -O2 plasma	17	37
80º- Ar plasma	23	32
80º Ar:O2 plasma (100:5)	17	30
80º Ar:O2 plasma (100:15)	18	31

Additional differences in surface topography between the OAD and OAD plasma assisted thin films can be also deduced from a detailed analysis of their normal SEM micrographs showing that at the surface of the plasma assisted films the nanocolumns are interconnected in the form of extended bundles (see Figures 2, 3 and supporting information S2). This visual assessment is confirmed by the 2D Fourier transform (FFT) plots of these images reported as insets in Figures 2 and 3 that depict an asymmetric shape for the plasma OAD thin films, but a symmetric rounded shape for the 80º thin films deposited in the absence of plasma. This difference sustains that in the plasma assisted films the surface grains are associated in the form of bundles along a

preferential direction perpendicular to the incoming material flux. A similar conclusion can be gained by looking to the topographic AFM profiles along these two perpendicular directions. The comparison between the line profiles of the 80º OAD and the 80º OAD O_2 plasma assisted films along two perpendicular directions clearly confirms the existence of a preferential bundling association direction of nanocolumns in the latter case (see supporting information S3) .

Chemistry, crystalline structure and porosity

E-beam evaporation of complex materials like ITO may induce changes in stoichiometry due to the preferential evaporation of one of the components. The "as-prepared" ITO thin films deposited in the absence of plasma were amorphous when examined by X-ray diffraction and presented a dark coloration indicating a certain lack of oxygen with respect to the stoichiometric mixed oxide. The plasma assisted films, although also amorphous, were less dark when their growth was assisted with a plasma of oxygen (or mixtures oxygen plus argon). As evidenced by SEM analysis, after annealing in O_2 at 350ºC for 6 hours all the OAD ITO films became transparent and crystalline and kept a microstructure similar to that of the original samples (see Supporting information S4). The X-ray diagrams of the annealed samples reported in Figure 6 are characterized by well defined peaks attributed to ITO (see for comparison the equivalent diagram for the commercial ITO film) and, in the case O_2 or mixtures of O_2/Ar plasma assisted films, some small peaks due to SnO_2. This minority segregation of tin oxide did not significantly affect the conductivity or optical properties of the films (see below) and no further discussion will be carried out here on this question.
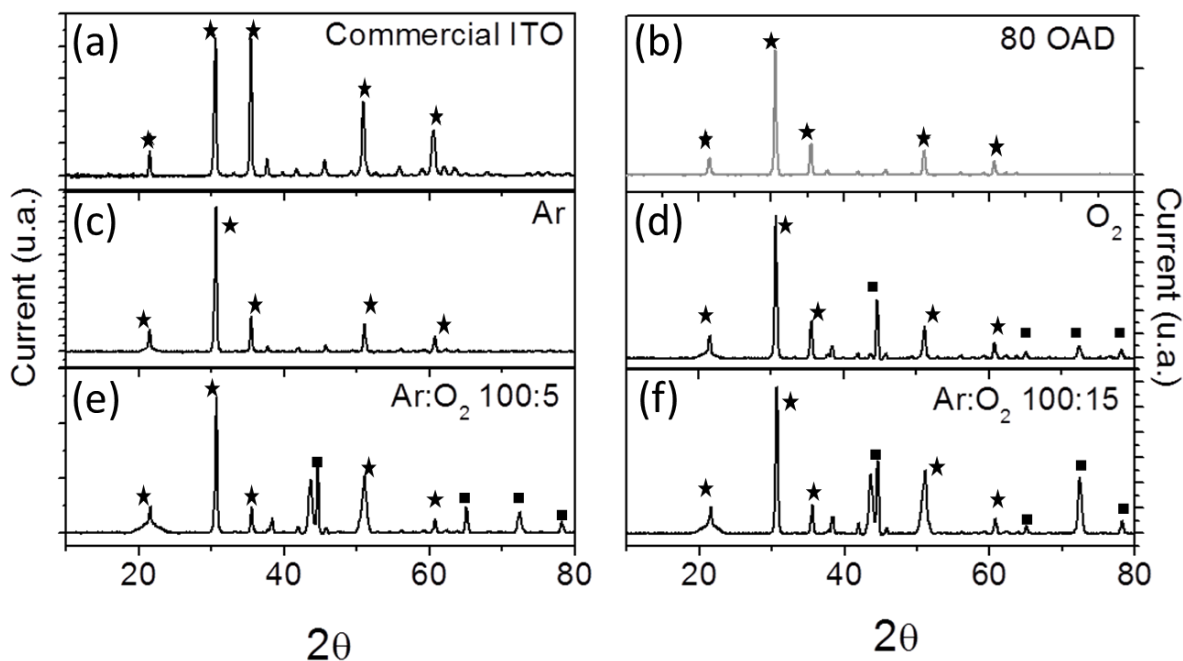
Figure 6. XRD diagrams of the ITO thin films after their annealing in oxygen at 350º. (a) Commercial ITO included for comparison. (b)-(f) diagrams of OAD and OAD plasma assisted thin films as indicated. Peaks highlighted with a star correspond to crystalline ITO, those denoted with squares to a SnO2 segregated phase.

The O/(In+Sn) atomic ratio and the elemental depth distribution of the films were determined by RBS (the corresponding spectra are reported as supported information S5). The results of this analysis (see Table 3) show that the relative content of oxygen is higher in the plasma assisted films and that it slightly increases after annealing, in agreement with the color bleaching induced by this treatment. The relatively higher content of oxygen determined for the plasma assisted film agrees with the enrichment in Sn deduced from the XRD diagrams (Figure 6) (in In_2O_3 the O:In ratio is 1.5, while it is 2 for SnO_2).

Table 3. Mass thickness, elemental percentages and ratios and density of OAD ITO thin films determined by RBS

Sample	Mass thickness (10^{15}at/cm^2)	[Sn]+[In] (%at)	[O] (%at)	[O]/ [Sn]+[In]	Density g/cm^3
ITO-80º	2250	39	61	1,56	3,7
ITO-80º/300ºC	2400	39	61	1,56	4,3
ITO –O2 plasma	2700	27	48	1,77	3,5
ITO-O2 plasma /300ºC	2400	32	59	1,84	3,9
ITO-Ar plasma	2700	30	55	1,83	3,8
ITO-Ar plasma/300ºC	2500	35	61	1,74	4,3
Commercial ITO	1450	39	61	1,56	7,2

Film densities were also determined by comparing their mass thicknesses obtained by RBS with the actual thicknesses estimated by direct observation of the cross section micrographs in Figures 2 and 3. In comparison with the density determined for the commercial ITO, the densities gathered in Table 3 for the OAD films are consistent with porosities of the order of 40-50% of their total volume, in good agreement with similar oxide thin films prepared by e-beam OAD.[19] It is also worth stressing that the pore volume remains almost unaltered by annealing, thus confirming that the microstructure does not significantly vary after this treatment (see supporting information 4).

Electrical conductivity

The annealed OAD films were transparent in the visible and presented a significant absorption in the near infrared, a typical characteristic attributed to a high concentration of free electrons in TCO materials.[1,2] To characterize the electrical transport properties of the OAD thin films we have measured their conductivity both at microscopic and macroscopic levels. The scanned conductivity maps reported in Figure 7 show that most surface features with a high conductivity roughly coincide with the protrusions observed in the topographic AFM images. This proves that in the OAD ITO thin films the in-depth conductivity mainly involves a preferential charge transport through the nanocolumns of the films. Moreover, the measured I-V curves at these sites reveal similar local conductivity values for the OAD and commercial ITO films and a transport pattern approaching an ohnmic behavior in all cases. Although the similar conductivities at microscopic level between the compact and OAD ITO films supports that the electronic characteristics of the examined materials are rather similar, this does not imply that their macroscopic conductivity should be similar too. Macroscopic cross-section and "sheet" conductivity measurements were carried out as described in the experimental section and the obtained I-V curves depicted a typical resistive Ohnmic behavior. The resistivity values reported in Table 4 show that the in-depth and sheet conductivities of the commercial ITO films used as reference are higher than those of the OAD ITO films, a difference that must be attributed to the smaller density and nanocolumnar microstructure of these samples.
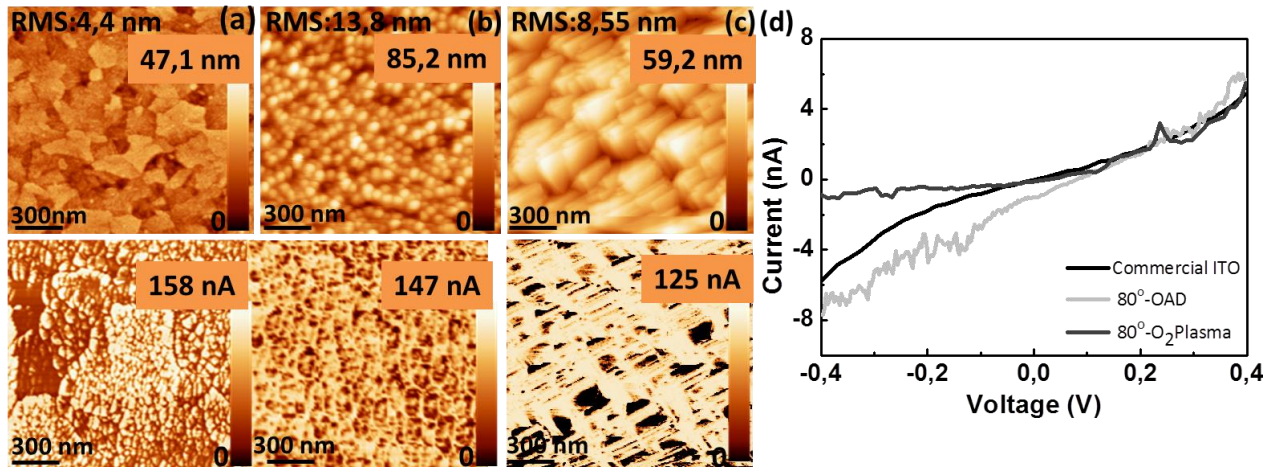
Figure 7. Topographic (top) and conductive scanning microscopy (down) images recorded for a commercial ITO film (a) and the indicated OAD thin films: 80º OAD (b) and 80º-O_2 plasma (c). The graphs in panel (d) correspond to I-V curves measured with the AFM tip placed on a position with a maximum conductivity.

Table 4. Sheet and in-depth resistivity values of OAD and OAD plasma assisted ITO films

Sample	In-depth resistivity (Ω*m)	Sheet resistivity (bundling direction) (Ω*sq)	Sheet resistivity (perpendicular direction) (Ω*sq)
Commercial ITO plate	6,3	2,1	2,2
80º -OAD	20,1	48,7	69,7
80º -O_2 Plasma	40,8	84,4	6624
80ºAr Plasma	19,5	55,5	123,1

In addition, while the sheet conductivities in the commercial ITO films are equivalent for two perpendicular surface directions, quite different conductivity values were determined in the plasma assisted films along the bundling and perpendicular directions. This difference proves that the bundling direction defines a preferential electrical pathway due to the lateral association

of nanocolumns and that these pathways are disrupted in the perpendicular direction. The difference is particularly worth noting for the O_2 plasma film where the resistivity in the direction perpendicular to the bundling direction is comparatively very high. To our knowledge no similar in-plane electrical anisotropy has been previously reported for other OAD thin films.

Surface anisotropy and fabrication of dichroic thin films

A typical application of ITO thin films consists of using them as electrodes for different purposes, including the development of sensors, nanoparticle deposition, etc.[49,50,61,62] Herein, we propose to exploit the bundling surface and conductivity anisotropies of the plasma assisted OAD thin films for the development of dichroic thin films. In previous works on plasmon anticounterfeiting films we proposed the use of OAD SiO_2 thin films as hosts or templates for, respectively, the fabrication of embedded anisotropic gold nanoparticles[50] or Ag surface nanostrips after evaporation and laser treatment.[49] The strategy proposed here consists of using the plasma assisted OAD ITO films as electrodes to directly deposit Au nanostructures with surface plasmon resonance activity.[49,50]

Electrochemical deposition of gold on the OAD ITO films leads to the formation of nanoparticles and/or nanostructures both on the film surface and in its interior. The normal and cross section SEM micrographs reported in Figure 8 show that small gold nanoparticles form on the surface of the 80º OAD-ITO film, mainly at the tip of the nanocolumns. A reduced number of nanoparticles also form in the interior of the film. By contrast, in the plasma assisted OAD ITO films, gold forms elongated aggregates in the hollow surface regions separating the nanocolumnar bundles, as well as in the pores separating these bundles in the interior of the films. The total amount of gold deposited in each case was similar and corresponded to

approximately $3{,}7*10^{15}$ atoms/cm^2 of gold as determined from the total current exchanged during the deposition process.
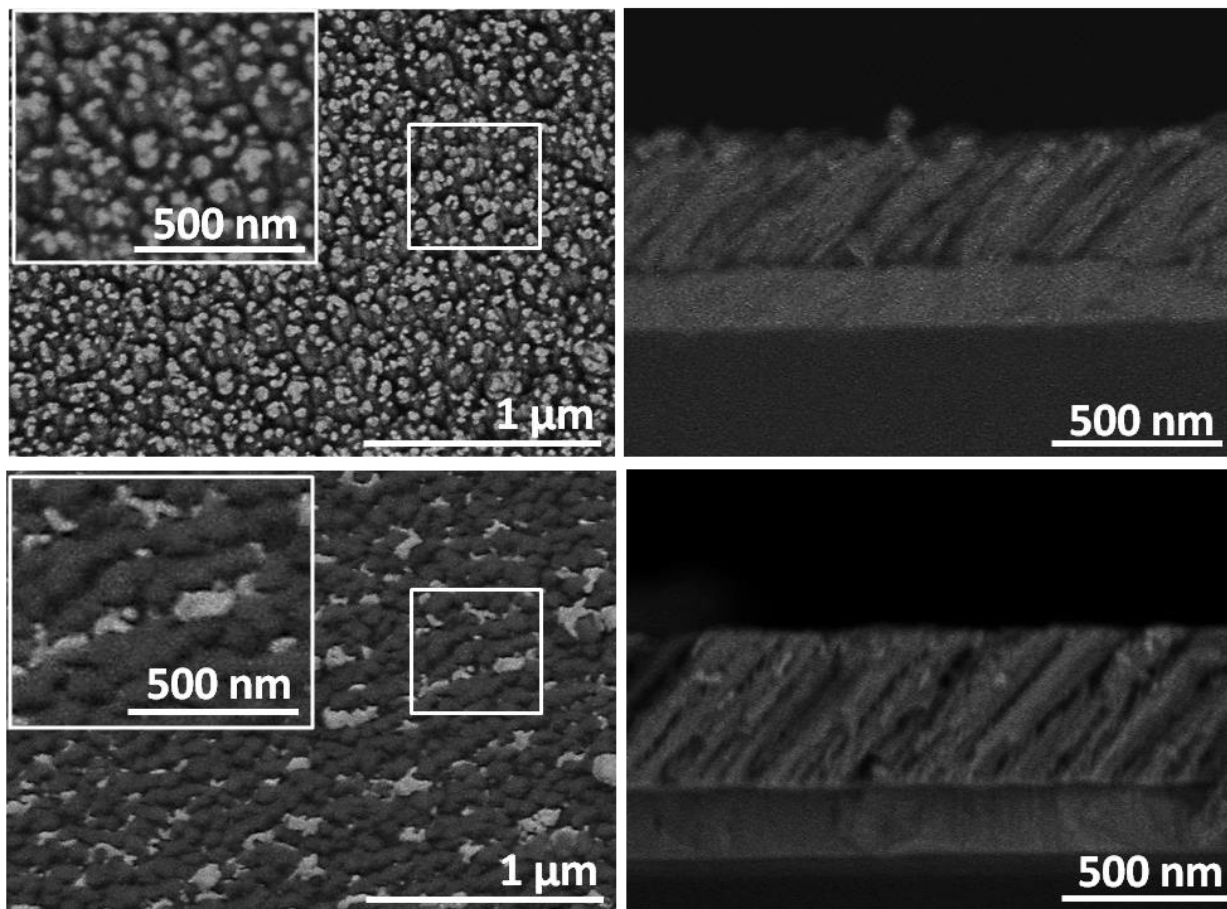

Figure 8. Normal (left) and cross section (right) SEM micrographs of 80º- OAD (top) and 80º-O$_2$ Plasma (down)ITO thin films after the electrochemical deposition of gold. The enlarged views included as insets in the normal SEM micrographs show the different shape of the gold aggregated formed on the surface of these two types of thin films.

The different distribution of gold in the two kinds of ITO films yields two types of surface plasmon resonances. Figure 9 shows the UV-vis spectra recorded with linearly polarized light for two azimuthal orientations of the films defined along the bundling direction in the plasma assisted OAD films (0º polarization) or the perpendicular to it (90º polarization). For these two

orientations, the spectra of the evaporated ITO films depict a similar absorption band at 535 nm attributed to the surface plasmon resonance of the electrochemically deposited gold nanoparticles.[49,50,63,64] Conversely, in the plasma assisted film, azimuthally turning the sample leads to significant changes in the absorption spectra. At 0º, the spectrum is characterized by a well defined resonance peak at 520 nm, while at 90º it depicts a less resolved structure where two broad and little resolved bands at 580 nm and 700 nm can be seen. This change renders a clear variation in the color of the sample as evidenced by the photographs shown in the Figure. A similar behavior has been reported in previous studies on anisotropic gold nanoparticles embedded in OAD SiO$_2$ thin films.[48] This dichroic behavior can be attributed to a different plasmon resonance response when aligning the polarization vector of the light along the longest or shortest dimensions of the gold nanostructures.[65]
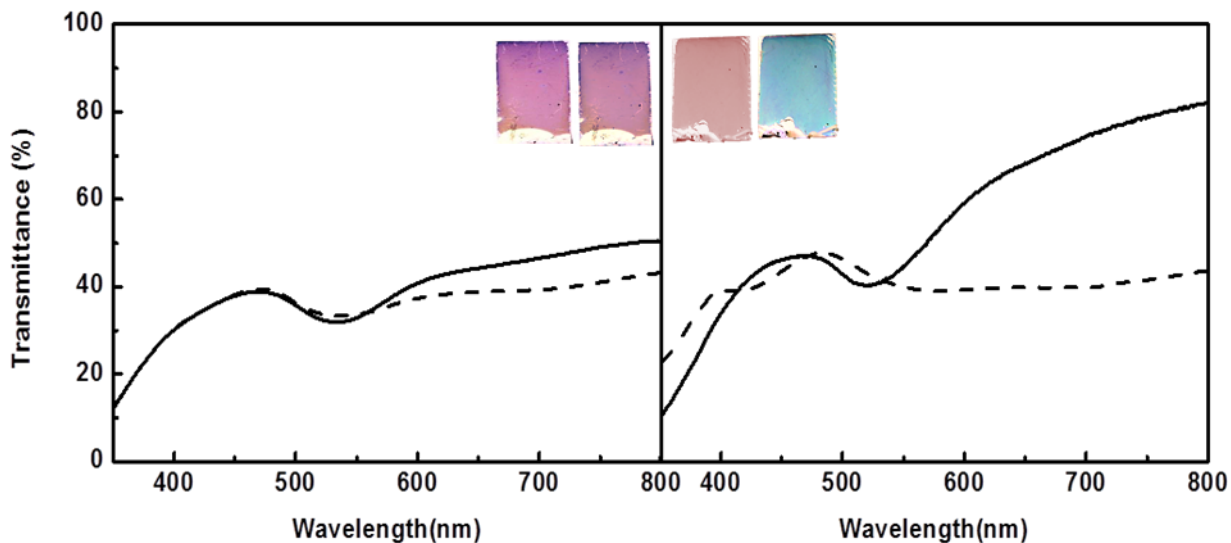

Figure 9. UV-vis transmittance spectra recorded with linearly polarized light 0º (dashed line) and 90º (full line) for gold electrochemically deposited on a 80º OAD ITO (left) and 80º-O2

Plasma ITO (right). The images clearly show the different aspect of the films examined with the two orientations of the polarized light.

DISCUSSION

Although well identified in the literature of OAD thin films[15,16], the bundling association of nanocolumns has been neither sufficiently explained nor exploited to get new complex nanostructures. In general, it is more common in metals[17] than in oxides[13,19,20] and therefore it seems associated with the different mobility and/or trapping probability of the species impinging onto the growing films. In a recent discussion about the heuristic "tangent rule"[44] relating the tilting angle of the nanocolumns (β) with the zenithal evaporation angle (α) we have proposed that this dependence can be explained by assuming that the deposition particles flying close to the surface can be trapped before impinging onto it. Such a trapping mechanism would cast an effective shadowing behind the growing nanostructures that would depend on an effective "trapping parameter" different for each material. Using a Monte Carlo simulation model, we demonstrated that β decreases for higher trapping probabilities, having a value of approximately 0.3 for OAD ITO. The decrease in the tilting angle found here for the plasma assisted OAD films would imply an increase in this parameter to a value close to one. Although the reasons accounting for this increase in the surface trapping probability in the presence of a plasma still require an specific investigation, we can anticipate that the electrical field associated to the sheath formed on the surface of the growing film exposed to the plasma[66] must be a critical factor enhancing the trapping probability of the deposition particles.

Besides a change in the nanocolumnar orientation, the morphological analysis of the plasma assisted films are characterized by an enhancement in the bundling association of the

23

nanocolumns. The hypothesis of an enhancement of the trapping probability under the action of the plasma can also explain the development of bundling since this phenomenon would not only occur at the nanocolumn tips but also at their sides, whereby favoring their lateral growth and association.

Similarly to other OAD metal oxides prepared at room temperature where only pure ballistic deposition processes are involved[1], the "as-deposited" ITO samples were amorphous. To get transparency in the visible, absorption in the NIR and electrical conductivity, the films were annealed in air at 350ºC, a treatment that produces their crystallization and complete oxidation. The crystalline OAD ITO films presented sheet and in-depth conductivities that differ from those of dense ITO films, a difference that has been related to their microstructure formed by tilted and separated nanocolumns. Distinct in-depth and sheet electrical conductivities have been reported for a wide variety of thin film materials[67,68] characterized by a different arrangement of the microstructural or molecular units in-depth or laterally. The additional in-plane anisotropy found in the plasma assisted OAD ITO thin films is an outstanding new feature that we have linked with the association of nanocolumns in the form of bundles and the definition of separated conductivity path-ways along them. The prospects of use of this feature are enormous and in the present work we have exploited a first possibility consisting of the electrochemical fabrication of dichroic films based on the surface plasmon resonance response of gold nanostructures. The different shape of the deposited aggregates found on the OAD and OAD plasma assisted ITO films must be related with local variations in the electrical potential at the surface. On OAD thin films the homogenous distribution of equally sized and round nanoparticles formed on the tips of the nanocolumns (cf. Figure 8) must be associated with an enhancement of the electrical field at these sites. In the plasma assisted OAD thin films, gold does not become deposited on the

hillocks of the surface nanostructures but rather in the space between bundles with an important tendency to grow in the interior of the films (cf. Figure 8). Clearly, this distinct deposition behavior must be linked with a blurring and homogenization of the electrical field along the bundles and the subsequent lost of the tip enhancement of electrical field.

CONCLUSIONS

The previous results and discussion have shown that the microstructure of OAD ITO thin films can be modified by exposing the growing films to a plasma. The observed decrease in the tilting angle and the bundling association of nanocolumns have been attributed to a higher trapping probability of the evaporated particles along their trajectory in the vicinity of the film. Both the OAD and the plasma assisted OAD ITO films present different in-depth and sheet conductivities as expected for their porous and nanocolumnar structure. In addition, the anisotropic in-plane conductivity behavior found in the plasma assisted samples has been associated with the definition of preferential conductivity tracks along the bundling direction of nanocolumns. The surface anisotropy of these samples has been utilized in the present work for the electrochemical deposition of elongated gold nanoparticles. The obtained composite films present a dichroic behavior when examined with polarized light. It is expected that these anisotropic thin films can be used for other applications where transparency and in-plane electrical anisotropy are relevant issues.

ASSOCIATED CONTENT

Supporting Information. Figures S1, S2, S3, S4 and S5. "This material is available free of charge via the Internet at http://pubs.acs.org."

AUTHOR INFORMATION

Corresponding Author

* e-mail: arge@icmse.csic.es

Author Contributions

The manuscript was written through contributions of all authors. All authors have given approval to the final version of the manuscript.

Notes

Any additional relevant notes should be placed here.

REFERENCES

(1)   Granqvist, C. G.; Hultåker, A. *Thin Solid Films* 2002, *411*, 1–5.

(2)   Kumar, A.; Zhou, C. *ACS Nano* 2010, *4*, 11–14.

(3)   Sunde, T. O. L.; Garskaite, E.; Otter, B.; Fossheim, H. E.; Sæterli, R.; Holmestad, R.; Einarsrud, M.-A.; Grande, T. *J. Mater. Chem.* 2012, *22*, 15740–15749.

(4)   Wang, T.; Radovanovic, P. V. *J. Phys. Chem. C* 2011, *115*, 406–413.

(5)   Kim, S. I.; Jung, T. D.; Song, P. K. *Thin Solid Films* 2010, *518*, 3085–3088.

(6)   Jung, Y. S.; Lee, S. S. *J. Cryst. Growth* 2003, *259*, 343–351.

(7)   Ikenoue, T.; Sakamoto, S.; Inui, Y. *Phys. Status Solidi C* 2014, *11*, 1237–1239.

(8)   Ali, H. M.; Mohamed, H. A.; Mohamed, S. H. *Eur. Phys. J. Appl. Phys.* 2005, *31*, 87–93.

(9)   Sood, A. W.; Poxson, D. J.; Mont, F. W.; Chhajed, S.; Cho, J.; Schubert, E. F.; Welser, R. E.; Dhar, N. K.; Sood, A. K. *J. Nanosci. Nanotechnol.* 2012, *12*, 3950–3953.

(10)   Zhong, Y.; Shin, Y. C.; Kim, C. M.; Lee, B. G.; Kim, E. H.; Park, Y. J.; Sobahan, K. M. A.; Hwangbo, C. K.; Lee, Y. P.; Kim, T. G. *J. Mater. Res.* 2008, *23*, 2500–2505.

(11)   Rider, D. A.; Tucker, R. T.; Worfolk, B. J.; Krause, K. M.; Lalany, A.; Brett, M. J.; Buriak, J. M.; Harris, K. D. *Nanotechnology* 2011, *22*, 085706.

(12)   Van Dijken, J. G.; Brett, M. J. *J. Vac. Sci. Technol. Vac. Surf. Films* 2012, *30*, 040606.

(13)   Leem, J. W.; Yu, J. S. *Opt. Express* 2011, *19 Suppl 3*, A258–A268.

(14)   Van Kranenburg, H.; Lodder, C. *Mater. Sci. Eng. R Rep.* 1994, *11*, 295–354.

(15)   Hawkeye, M. M.; Taschuk, M. T.; Brett, M. J. *Glancing angle deposition of thin films: engineering the nanoscale*; 2014.

(16)   Hawkeye, M. M.; Brett, M. J. *J. Vac. Sci. Technol. Vac. Surf. Films* 2007, *25*, 1317.

(17)   Chen, L.; Lu, T.-M.; Wang, G.-C. *J. Appl. Phys.* 2012, *112*, 024303.

(18)   Hara, K.; Kamiya, M.; Hashimoto, T.; Okamoto, K.; Fujiwara, H. *Thin Solid Films* 1988, *158*, 239–244.

(19)   González-García, L.; Parra-Barranco, J.; Sánchez-Valencia, J. R.; Barranco, A.; Borrás, A.; González-Elipe, A. R.; García-Gutiérrez, M.-C.; Hernández, J. J.; Rueda, D. R.; Ezquerra, T. A. *Nanotechnology* 2012, *23*, 205701.

(20)   Schulz, U.; Terry, S. G.; Levi, C. G. *Mater. Sci. Eng. A* 2003, *360*, 319–329.

(21)   Wang, S.; Xia, G.; He, H.; Yi, K.; Shao, J.; Fan, Z. *J. Alloys Compd.* 2007, *431*, 287–291.

(22) Basnet, P.; Larsen, G. K.; Jadeja, R. P.; Hung, Y.-C.; Zhao, Y. *ACS Appl. Mater. Interfaces* 2013, *5*, 2085–2095.

(23) Merkel, J. J.; Sontheimer, T.; Rech, B.; Becker, C. *J. Cryst. Growth* 2013, *367*, 126–130.

(24) Ehsani, M. H.; Rezagholipour Dizaji, H.; Azizi, S.; Ghavami Mirmahalle, S. F.; Hosseini Siyanaki, F. *Phys. Scr.* 2013, *88*, 025602.

(25) Yang, B.; Duan, H.; Zhou, C.; Gao, Y.; Yang, J. *Appl. Surf. Sci.* 2013, *286*, 104–108.

(26) González-García, L.; González-Valls, I.; Lira-Cantu, M.; Barranco, A.; González-Elipe, A. R. *Energy Environ. Sci.* 2011, *4*, 3426–3435.

(27) Oliva-Ramirez, M.; González-García, L.; Parra-Barranco, J.; Yubero, F.; Barranco, A.; González-Elipe, A. R. *ACS Appl. Mater. Interfaces* 2013, *5*, 6743–6750.

(28) He, Y.; Zhao, Y. *Nanoscale* 2011, *3*, 2361.

(29) Martin, P. M. *Handbook of deposition technologies for films and coatings science, applications and technology*; Elsevier: Amsterdam; Boston, 2010.

(30) Parra-Barranco, J.; Oliva-Ramirez, M.; Gonzalez-Garcia, L.; Alcaire, M.; Macias-Montero, M.; Borras, A.; Frutos, F.; Gonzalez-Elipe, A. R.; Barranco, A. *ACS Appl. Mater. Interfaces* 2014, *6*, 11924–11931.

(31) Schmidt, D.; Kjerstad, A. C.; Hofmann, T.; Skomski, R.; Schubert, E.; Schubert, M. *J. Appl. Phys.* 2009, *105*, 113508.

(32) Xi, J.-Q.; Schubert, M. F.; Kim, J. K.; Schubert, E. F.; Chen, M.; Lin, S.-Y.; Liu, W.; Smart, J. A. *Nat. Photonics* 2007, *1*, 176–179.

(33) Schubert, M. F.; Kim, J. K.; Chhajed, S.; Schubert, E. F. Ellison, M. J., Ed.; 2007; pp. 667403–667403 – 7.

(34) Kim, J. K.; Chhajed, S.; Schubert, M. F.; Schubert, E. F.; Fischer, A. J.; Crawford, M. H.; Cho, J.; Kim, H.; Sone, C. *Adv. Mater.* 2008, *20*, 801–804.

(35) Poxson, D. J.; Kuo, M.-L.; Mont, F. W.; Kim, Y.-S.; Yan, X.; Welser, R. E.; Sood, A. K.; Cho, J.; Lin, S.-Y.; Schubert, E. F. *MRS Bull.* 2011, *36*, 434–438.

(36) Yan, X.; Mont, F. W.; Poxson, D. J.; Cho, J.; Schubert, E. F.; Kim, M.-H.; Sone, C. *J. Appl. Phys.* 2011, *109*, 103113.

(37) Beaudry, A. L.; Tucker, R. T.; LaForge, J. M.; Taschuk, M. T.; Brett, M. J. *Nanotechnology* 2012, *23*, 105608.

(38) Tucker, R. T.; Beaudry, A. L.; LaForge, J. M.; Taschuk, M. T.; Brett, M. J. *Appl. Phys. Lett.* 2012, *101*, 193101.

(39) Taschuk, M. T.; Tucker, R. T.; LaForge, J. M.; Beaudry, A. L.; Kupsta, M. R.; Brett, M. J. *J. Appl. Phys.* 2013, *114*, 244304.

(40) Beaudry, A. L.; LaForge, J. M.; Tucker, R. T.; Li, P.; Taschuk, M. T.; Brett, M. J. *Cryst. Growth Des.* 2013, *13*, 212–219.

(41) Beaudry, A. L.; LaForge, J. M.; Tucker, R. T.; Sorge, J. B.; Adamski, N. L.; Li, P.; Taschuk, M. T.; Brett, M. J. *Nano Lett.* 2014, *14*, 1797–1803.

(42) Sorge, J. B.; Taschuk, M. T.; Wakefield, N. G.; Sit, J. C.; Brett, M. J. *J. Vac. Sci. Technol. A* 2012, *30*, 021507.

(43) Zhao, Y.; He, Y.; Brown, C. *Appl. Phys. Lett.* 2012, *100*, 033106.

(44) Alvarez, R.; Lopez-Santos, C.; Parra-Barranco, J.; Rico, V.; Barranco, A.; Cotrino, J.; Gonzalez-Elipe, A. R.; Palmero, A. *J. Vac. Sci. Technol. B* 2014, *32*, 041802.

(45) Sánchez-Valencia, J. R.; Blaszczyk-Lezak, I.; Espinós, J. P.; Hamad, S.; González-Elipe, A. R.; Barranco, A. *Langmuir* 2009, *25*, 9140–9148.

(46) Tait, R. N.; Smy, T.; Brett, M. J. *Thin Solid Films* 1993, *226*, 196–201.

(47) Sanchez-Valencia, J. R.; Toudert, J.; Borras, A.; Barranco, A.; Lahoz, R.; de la Fuente, G. F.; Frutos, F.; Gonzalez-Elipe, A. R. *Adv. Mater.* 2011, *23*, 848–853.

(48) Gonzalez-García, L.; Parra-Barranco, J.; Sanchez-Valencia, J. R.; Ferrer, J.; Garcia-Gutierrez, M.-C.; Barranco, A.; Gonzalez-Elipe, A. R. *Adv. Funct. Mater.* 2013, *23*, 1655–1663.

(49) Wang, L.; Mao, W.; Ni, D.; Di, J.; Wu, Y.; Tu, Y. *Electrochem. Commun.* 2008, *10*, 673–676.

(50) Ma, Y.; Di, J.; Yan, X.; Zhao, M.; Lu, Z.; Tu, Y. *Biosens. Bioelectron.* 2009, *24*, 1480–1483.

(51) Roth, S. V.; Döhrmann, R.; Dommach, M.; Kuhlmann, M.; Kröger, I.; Gehrke, R.; Walter, H.; Schroer, C.; Lengeler, B.; Müller-Buschbaum, P. *Rev. Sci. Instrum.* 2006, *77*, 085106.

(52) Alvarez, R.; García-Martín, J. M.; Macías-Montero, M.; Gonzalez-Garcia, L.; González, J. C.; Rico, V.; Perlich, J.; Cotrino, J.; González-Elipe, A. R.; Palmero, A. *Nanotechnology* 2013, *24*, 045604.

(53) González-García, L.; Barranco, A.; Páez, A. M.; González-Elipe, A. R.; García-Gutiérrez, M.-C.; Hernández, J. J.; Rueda, D. R.; Ezquerra, T. A.; Babonneau, D. *ChemPhysChem* 2010, *11*, 2205–2208.

(54) Gil-Rostra, J.; Chaboy, J.; Yubero, F.; Vilajoana, A.; González-Elipe, A. R. *ACS Appl. Mater. Interfaces* 2013, *5*, 1967–1976.

(55) Kanno, Y.; Suzuki, T.; Yamauchi, Y.; Kuroda, K. *J. Phys. Chem. C* 2012, *116*, 24672–24680.

(56) Dudin, P. V.; Unwin, P. R.; Macpherson, J. V. *J. Phys. Chem. C* 2010, *114*, 13241–13248.

(57) Palik, E. D. *Handbook of Optical Constants of Solids*; Academic Press, 2012.

(58) Pillai, P. P.; Pacławski, K.; Kim, J.; Grzybowski, B. A. *Adv. Mater.* 2013, *25*, 1623–1628.

(59) Fractal Concepts in Surface Growth | Condensed matter physics, nanoscience and mesoscopic physics,2014

(60) Karabacak, T.; Singh, J.; Zhao, Y.-P.; Wang, G.-C.; Lu, T.-M. *Phys. Rev. B* 2003, *68*.

(61) Schaming, D.; Renault, C.; Tucker, R. T.; Lau-Truong, S.; Aubard, J.; Brett, M. J.; Balland, V.; Limoges, B. *Langmuir* 2012, *28*, 14065–14072.

(62) Kasik, I.; Mrazek, J.; Podrazky, O.; Seidl, M.; Aubrecht, J.; Tobiska, P.; Pospisilova, M.; Matejec, V.; Kovacs, B.; Markovics, A.; Szili, M. *Sens. Actuators B Chem.* 2009, *139*, 139–142.

(63) Chourou, M. L.; Fukami, K.; Sakka, T.; Ogata, Y. H. *Phys. Status Solidi C* 2011, *8*, 1783–1786.

(64) Sakai, N.; Fujiwara, Y.; Arai, M.; Yu, K.; Tatsuma, T. *J. Electroanal. Chem.* 2009, *628*, 7–15.

(65) Murray, W. A.; Barnes, W. L. *Adv. Mater.* 2007, *19*, 3771–3782.

(66) Conrad, J. R.; Radtke, J. L.; Dodd, R. A.; Worzala, F. J.; Tran, N. C. *J. Appl. Phys.* 1987, *62*, 4591–4596.

(67) Yan, H.; Park, S. H.; Finkelstein, G.; Reif, J. H.; LaBean, T. H. *Science* 2003, *301*, 1882–1884.

(68) Zhang, M.; Fang, S.; Zakhidov, A. A.; Lee, S. B.; Aliev, A. E.; Williams, C. D.; Atkinson, K. R.; Baughman, R. H. *Science* 2005, *309*, 1215–1219.